Engineering Notes

Dynamics-Based Loads Monitoring Algorithm for Onboard Commercial Aircraft Usage

Georgios Ntourmas* and Rene Meissner†
Airbus, 21129 Hamburg, Germany
and
Vasilios Spitas‡
National Technical University of Athens, 15780 Athens, Greece

https://doi.org/10.2514/1.C035768

I. Introduction

A LOADS monitoring algorithm (LMA) uses data acquired by sensors placed on the aircraft to estimate potential high load exceedances. The LMA examined in this paper needs to be able to run on real-time onboard the available computers of a typical today's aircraft. What is more, the current study focuses on high load events occurring during in-flight operation and more specifically the ones caused by severe turbulence encounters, extreme maneuvering, or a combination of those. The need for accurate LMAs stems from the fact that false alarms unnecessarily ground the aircraft, increasing operational costs due to schedule interruption.

The complexity and accuracy of the delivered LMA are bounded by the limited computational resources as well as from available measurements from the sensors and their equivalent sampling rates. These constraints render existing approaches either not accurate or robust enough, or too complex to be implemented on the aircraft.

Traditionally, simplified solutions based on the aircraft's flight envelope are used to warn about potential load exceedances [1,2]. Recently, increased computational resources and sensor availability have enabled more accurate and direct implementations [3].

Aircraft structural loads depend on many factors and require complex computer simulations in order to be calculated. Hence, many approaches followed in the past have focused on machine learning and data-driven approaches [4–15] to describe loads based on the different parameters that affect them in a way simplified enough for real-time usage. The previous approaches are potentially feasible from the computational limitation point of view, but in general, do not produce accurate results when presented with cases that differ significantly to the ones that were used for training.

In contrast to data-driven approaches, physics-based approaches that model the structural loads on the aircraft have also been attempted. Besides sophisticated aeroelastic models used for the design of an aircraft, simplified lightweight models aimed for early design phases or optimization have also been developed [16–20]. Unfortunately, such models are geared toward calculation of loads based on defined, isolated maneuvers or gusts, which is not the case during real aircraft operation.

The developed methodology aimed to overcome the disadvantages of data-driven methodologies and present a physics-based approach that is computationally light enough to be implemented onboard the available systems of an already instrumented commercial aircraft. A time-domain simulation using a decoupled structural and simplified aerodynamic model of the aircraft is presented. The formulation of the problem is indirect to better exploit the sampling rate of the built-in, onboard available sensors. A simplification procedure allowing the development of a lightweight LMA based on the previously mentioned time-domain simulation is demonstrated. Finally, the validity of the results obtained is demonstrated by comparison with reference data.

II. Methodology

Prior to concluding to the LMA is to develop a simulation environment able to assess the inputs from the aircraft sensors and calculate the resulting structural loads on the airframe. Because of the limiting computational resources available onboard, different simple sample cases have to be run beforehand resulting in the creation of a loads database. Results produced and trends observed in the database shall then be embodied in a simplified way in the final LMA named Flight Overload Real Time Identification Algorithm (FORTIA), providing a quick estimation of structural limit loads during in-service operation.

A. Simulation Environment

An available sensor that is highly sampled is the vertical acceleration of the aircraft measured near the center of gravity. This sensor is selected as the basis of the developed simulation regarding the computation of the dynamic loads. High-fidelity aeroelasticity models are used by the industry to calculate structural loads for different operating conditions. Such models use the definition of a maneuver or gust case as an input and calculate the external forces applied on the structure by deriving all the necessary parameters (angle of attack, control surface deflections, etc.). The developed model follows an indirect approach to the solution of the equations of motion because some of the needed parameters are not available or are available at an insufficient sampling rate.

The equations of motion for a linear vibrating model with n degrees of freedom are defined by Eq. (1) [21]:

$$\boldsymbol{M}\ddot{\boldsymbol{x}} + \boldsymbol{C}\dot{\boldsymbol{x}} + \boldsymbol{K}\boldsymbol{x} = \boldsymbol{F}_{\text{ex}} \tag{1}$$

In Eq. (1), $\boldsymbol{M}, \boldsymbol{C}, \boldsymbol{K} \in \mathbb{R}^{nxn}$ stand for the physical mass, damping, and stiffness matrices of the structural model, respectively. The displacement vector is denoted by $\boldsymbol{x} \in \mathbb{R}^{nx1}$, and $\boldsymbol{F}_{\text{ex}} \in \mathbb{R}^{nx1}$ is the vector of the external forces exerted on the structure.

It is first assumed that the aircraft is free to vibrate under the actuation of a concentrated force vector exerted on a specific node of the structural model lying in the vicinity of the accelerometer and the center of mass of the aircraft, along with distributed gravitational forces. This vector of external concentrated forces is calculated from the measured accelerations. Any acceleration measured at the center of mass of the aircraft is linked to a real force acting on the plane.

Equation (1) needs to be rearranged into Eq. (2) to account for this indirect approach to the dynamics of the aircraft:

Received 16 October 2019; revision received 4 May 2020; accepted for publication 5 May 2020; published online 28 May 2020.

*Kreetslag 10; also Diploma Thesis Student, School of Mechanical Engineering, National Technical University of Athens, Heroon Polytechniou 9, Zografou, 15780 Athens, Greece; currently Ph.D. Candidate, University of Nottingham, NG7 2RD, Nottingham, U.K. Student Member AIAA.

†Loads and Aeroelastics Engineer, Airbus Loads and Aeroelasticity, Kreetslag 10.

‡Assistant Professor, School of Mechanical Engineering, Heroon Polytechniou 9, Zografou.

$$\boldsymbol{M_c}\ddot{\boldsymbol{x}}_{\boldsymbol{c}} + \boldsymbol{C_c}\dot{\boldsymbol{x}}_{\boldsymbol{c}} + \boldsymbol{K_c}\boldsymbol{x_c} = \boldsymbol{F_c} \tag{2}$$

In Eq. (2), the subscript c stands for concentrated forces. After rearranging the terms, the modified vector of unknown reactions $\ddot{\boldsymbol{x}}_{\boldsymbol{c}}$ contains three forces acting on the node, where the accelerations are given as input [Eq. (3)]:

$$\ddot{\boldsymbol{x}}_{\boldsymbol{c}} = [\,\ddot{x}_1 \quad \cdots \quad F_x \quad F_y \quad F_z \quad \ddot{x}_i \quad \cdots \quad \ddot{x}_n\,]^T \tag{3}$$

The x axis of the Cartesian coordinate system used, points opposite to the acceleration of gravity in level flight, whereas the y axis is parallel to the freestream. The mass, stiffness, damping, and external force matrices have to be modified accordingly:

$$\boldsymbol{M_c} = \begin{bmatrix} M_{11} & & 0 & 0 & 0 & & \\ \vdots & \ddots & \cdots & \cdots & \cdots & \cdots & \cdots \\ & & -1 & 0 & 0 & & \\ & & 0 & -1 & 0 & & \\ & & 0 & 0 & -1 & M_{(i-1)i} & \\ \vdots & \vdots & \vdots & \vdots & \vdots & \ddots & \cdots \\ & & 0 & 0 & 0 & & M_{(i-1)i} \end{bmatrix} \tag{4}$$

$$\boldsymbol{K_c} = \begin{bmatrix} K_{11} & & 0 & 0 & 0 & & \\ \vdots & \ddots & \cdots & \cdots & \cdots & \cdots & \cdots \\ & & 0 & 0 & 0 & & \\ & & 0 & 0 & 0 & & \\ & & 0 & 0 & 0 & K_{(i-1)i} & \\ \vdots & \vdots & \vdots & \vdots & \vdots & \ddots & \cdots \\ & & 0 & 0 & 0 & & K_{nn} \end{bmatrix} \tag{5}$$

The damping matrix $\boldsymbol{C_c}$ is formulated similarly to the stiffness matrix. Finally, the right-hand-side known vector $\boldsymbol{F_c}$ of Eq. (2) becomes

$$\boldsymbol{F_c} = [\boldsymbol{0} - \boldsymbol{M}_{nx3}\ddot{\boldsymbol{x}}_{\text{input}} - \boldsymbol{C}_{nx3}\ddot{\boldsymbol{x}}_{\text{input}} - \boldsymbol{K}_{nx3}\boldsymbol{x}_{\text{input}}]^T \tag{6}$$

where $\ddot{\boldsymbol{x}}_{\text{input}} \in \mathbb{R}^{3\times 1}$ contains the measured accelerations, and $\boldsymbol{M}_{nx3}$, $\boldsymbol{C}_{nx3}$, and $\boldsymbol{K}_{nx3}$ are the parts of the original mass, damping, and stiffness matrices missing from the matrices introduced in Eq. (2).

Such a simplified approach does not produce structural loads that are accurate enough because the distribution of the aforementioned concentrated forces across the aircraft structure is not taken into account. Hence, the need to model all basic aerodynamic forces on the aircraft rises.

Aerodynamic forces exerted on an aircraft depend on various factors, such as the flow conditions, the aircraft's control surface deflections, and aeroelastic effects. Different numerical methods can be employed to accurately calculate these effects [22–24]. In industry, extensive wind-tunnel testing has been conducted and all basic aerodynamic effects have been modeled. Therefore, the chosen aerodynamic modeling for the simulation environment developed is based on these available data, as they provide excellent accuracy with minimal computational effort and design complexity.

For the sake of simplicity, only forces acting in the vertical direction of the aircraft were modeled. As stated earlier, the number of inputs and more specifically the time variant inputs need to be kept low. Thus, the aerodynamic model introduced bears a lot of simplifications and is built in such a way that no other time variant input is required.

Simply stated, the aerodynamic forces on the aircraft hold a predefined constant distribution, and the angle of attack, which is internally calculated in the system of equations, regulates the exact amplitude of the forces, such that the measured accelerations are met.

The assumptions made regarding the aerodynamic model are

1) Mach number and dynamic pressure are considered constant during a suspected overload event.

2) No control surface deflections are taken into account.

3) The high lift (flap and slat) configuration and the mass distribution of the aircraft remain constant. In this modeling, zero flap and slat angles are assumed.

4) The angle of attack is the same for all lift-producing surfaces except for the horizontal tailplane (HTP), which is also affected by the downstream angle of attack.

5) All aerodynamics are considered steady and no aeroelastic effects are modeled.

The lift force L for a body exposed at a flow of dynamic pressure q is given by Eq. (7):

$$L = q\left(\frac{dC_L}{da}a + C_{L0}\right)S \tag{7}$$

In Eq. (7), dC_L/da stands for the slope of the lift curve with respect to the angle of attack a, C_{L0} is the lift coefficient of the surface at zero angle of attack, and S is the reference surface of the lifting body. The surfaces whose lift is accounted for in the current model are the wings, fuselage, HTP, pods, and winglets.

The angle of attack used for all of the aforementioned surfaces is the same except for the HTP for which the angle of attack is given by

$$a_{\text{HTP}} = a - \varepsilon \tag{8}$$

where ε is the downwash angle calculated as

$$\varepsilon = \varepsilon_0 + \frac{d\varepsilon}{da}a \tag{9}$$

In Eq. (9), ε_0 is the zero angle-of-attack downwash angle, and $d\varepsilon/da$ is the slope of the downwash angle with respect to the angle of attack.

Assuming a constant, known Mach number and a time-invariant configuration and neglecting control surfaces deflected, the aerodynamic data can be extracted and interpolated on the grid of nodes of the structural model. Finally, by assuming a common, global dynamic pressure for all lift-producing surfaces on the aircraft, the aerodynamic lift can be calculated as a function of the angle of attack.

Equation (2) can now be rewritten as

$$\boldsymbol{M_a}\ddot{\boldsymbol{x}}_{\boldsymbol{a}} + \boldsymbol{C_a}\ddot{\boldsymbol{x}}_{\boldsymbol{a}} + \boldsymbol{K_a}\boldsymbol{x_a} = \boldsymbol{F_a} \tag{10}$$

The subscript a in Eq. (10) stands for aerodynamic forces, because the aerodynamic model is introduced in this set of equations. Now, the vector of unknown reactions contains the angle of attack in place of the concentrated force acting in the vertical direction:

$$\ddot{\boldsymbol{x}}_{\boldsymbol{a}} = [\,\ddot{x}_1 \quad \cdots \quad a \quad F_y \quad F_z \quad \ddot{x}_i \quad \cdots \quad \ddot{x}_n\,]^T \tag{11}$$

The other two concentrated forces still remain as unknown and are assumed decoupled from the vertical component:

$$\boldsymbol{M_a} = \begin{bmatrix} M_{11} & & -L_1 & 0 & 0 & & \\ \vdots & \ddots & \cdots & \cdots & \cdots & \cdots & \cdots \\ & & -L_{(i-3)} & 0 & 0 & & \\ & & -L_{(i-2)} & -1 & 0 & & \\ & & -L_{(i-1)} & 0 & -1 & M_{(i-1)i} & \\ \vdots & \vdots & \vdots & \vdots & \vdots & \ddots & \cdots \\ & & -L_n & 0 & 0 & & M_{nn} \end{bmatrix} \tag{12}$$

The modified stiffness and damping matrices remain the same as in Eq. (2):

$$\boldsymbol{C}_a = \boldsymbol{C}_c$$
$$\boldsymbol{K}_a = \boldsymbol{K}_c \tag{13}$$

The right-hand side of the equations now includes the known gravitational forces and the part of the aerodynamic forces that are independent of the angle of attack:

$$\boldsymbol{F_a} = [\boldsymbol{0} - \boldsymbol{M}_{nx3}\ddot{\boldsymbol{x}}_{\text{input}} - \boldsymbol{C}_{nx3}\ddot{\boldsymbol{x}}_{\text{input}} - \boldsymbol{K}_{nx3}\boldsymbol{x}_{\text{input}} - \boldsymbol{F}_{\text{grav}} + \boldsymbol{F}_{\text{aero\_const}}]^T \tag{14}$$

The system of equations is solved in Simulink® using ode23tb, which is a differential equation solver for stiff systems of equations using the trapezoidal rule and a backward differentiation formula. Once the system of equations is solved, all external forces can be calculated knowing the angle of attack. To compute the structural loads on the aircraft, the flexible reactions ($\ddot{\boldsymbol{x}}_{\text{flex}}, \ddot{\boldsymbol{x}}_{\text{flex}}, \boldsymbol{x}_{\text{flex}}$) of each node need to be calculated, and then the modal equations of motion as described in Eq. (15) are solved:

$$m\ddot{p} + c\dot{p} + kp = f_{\text{ex}} \tag{15}$$

Equation (15) is derived by expressing the physical coordinates x of the system as $x = \Phi p$, where p is the modal coordinate vector of the system and Φ is the modal matrix from which only the flexible normal modes are used. The nodal loads can then be calculated as

$$\boldsymbol{P}_{\text{nodal}} = \boldsymbol{K}\boldsymbol{x}_{\text{flex}} \tag{16}$$

Once nodal loads are calculated, the actual structural loads (integrated loads) can be computed as in [25] using the available transformation matrix T. This procedure is common practice within Airbus, and so for the aircraft model used, a matrix transforming nodal loads to integrated loads already exists, such that

$$\boldsymbol{P}_{\text{integrated}} = \boldsymbol{T}\boldsymbol{P}_{\text{nodal}} \tag{17}$$

The resulting integrated load vector contains three forces and three moments for each node. Bearing in mind that the input forces for the model are just vertical forces, the integrated loads that contain useful information are mostly the vertical shear forces F_z and the bending moment along the axis that is normal to the examined component's reference axis. For the wing, that bending moment is M_x.

B. Simplifications and Loads Database

The developed simulation cannot be handled by the computer onboard the aircraft that is designated for the LMA; hence, simplifications must be introduced.

1. *Vertical Acceleration*

The LMA will need to be able to quickly assess the structural loads by matching the measured vertical acceleration to a case that has been precalculated on a computer able to run the simulation. The obvious problem that rises is that a time-dependent signal can have infinite different forms, amplitudes, etc. The problem needs to be discretized so that these infinite possible signals become a small finite number of inputs that will be fed in the simulation environment to create a loads database.

The assumption that was made is that each input vertical acceleration signal that will be run by the simulation is a simple sinusoidal waveform of $T/2$ duration with T being the period. Each waveform can be uniquely defined by an amplitude A and frequency f. The aforementioned assumption introduces the following limitation. The measured signals will never be as simple as sinusoidal waveforms, but they will have to be interpreted in such a way. Additionally, it is assumed that consecutive half-waves of different frequencies interfere in a destructive way to avoid calculating all different combinations that might exist.

Using the aforementioned assumptions, the loads at a station on the wing can be calculated as

$$P = \frac{dP}{dA}(f)A + P_{1g} \tag{18}$$

In Eq. (18), A stands for the amplitude of the waveform, f for the frequency, and P_{1g} for the $1g$ load level from gravity. The slope of the load quantity with respect to the amplitude dP/dA can be directly calculated using any two data points of different amplitudes and of the same frequency. Of course, this slope is frequency dependent.

Interpolation between the precalculated data points is further simplified by introducing a polynomial $(dP/dA)(f)$, which can be used onboard for the calculation of the loads. This method of calculation is used for all stations and vertical accelerations acting for less than $T/2$. Higher durations are treated as superposition of several $T/2$ constituents, because it is highly unlikely that smooth sinusoidal components will occur for longer than $T/2$ due to the stochastic nature of turbulence.

Considering the previous analysis, the relevant load quantities for each station can be calculated if a certain frequency and amplitude are given as inputs. Hence, a procedure that will be able to translate the vertical acceleration signal into simple sinusoidal waveforms of half a period duration, without requiring the mathematical rigor and complexity of Fourier techniques, must be created. First of all, two cutoff thresholds for the vertical load factor (i.e., the vertical acceleration in g, including gravity) are defined as $n_{z1} = 0.5$ and $n_{z2} = 1.5\ (1 \pm 0.5g)$. It is assumed that any load factor recorded with a value $n_{z1} \leq n_z \leq n_{z2}$ does not constitute a high load event. Whenever one of these two thresholds is exceeded, the slope of the vertical acceleration with respect to time is calculated at this specific time step. As long as this threshold is exceeded, the time steps are counted and also the current maximum vertical acceleration data point is stored. When the amplitude of the signal stops exceeding the threshold, the slope of the vertical acceleration with respect to time is calculated at that instant. Knowing the sampling frequency and the number of time steps for which the threshold was exceeded, the time above the threshold can be computed. To calculate the actual $T/2$ time of the signal, the two calculated slopes of the vertical acceleration with respect to time are used, assuming that the signal was following these slopes until reaching $1g$. Once the $T/2$ is calculated, the frequency can be also calculated and the amplitude is taken as the maximum vertical acceleration data point.

2. *Aircraft Mass and Mass Distribution*

The importance of the mass of the aircraft on the calculation of the structural loads has been demonstrated by Rokhsaz and Kliment [26] and Rokhsaz et al. [27]. One of the inputs to the simulation is a specific mass case (i.e., a specific mass matrix). Different mass cases represent different mass distributions and loading configurations of the aircraft. To minimize the complexity of the LMA, its only inputs are the total mass of the aircraft and the position of the center of gravity in the longitudinal axis of the aircraft. Using this information, the LMA applies the relevant coefficients in Eq. (18) to calculate the structural loads.

III. Results: Validation

During this section, the achieved accuracy of the simulation model will be assessed by comparing the time series results of the simulation developed against other time series data acquired from flight tests or high-fidelity aeroelastic models used for the design of the aircraft.

The first case that will be examined in comparison is an avoidance maneuver. During this maneuver, the pilot simultaneously commands high pitch and roll angles. As seen in Fig. 1, both the incremental bending moment and shear force match well, especially considering that the mass case used for the simulation cannot be a perfect match with the actual mass distribution of the aircraft.

In Fig. 2, a full sidestick maneuver is examined. The pilot inputs full stick commands making the aircraft roll to the left and right or vice versa. The shape of the two loads matches adequately for the

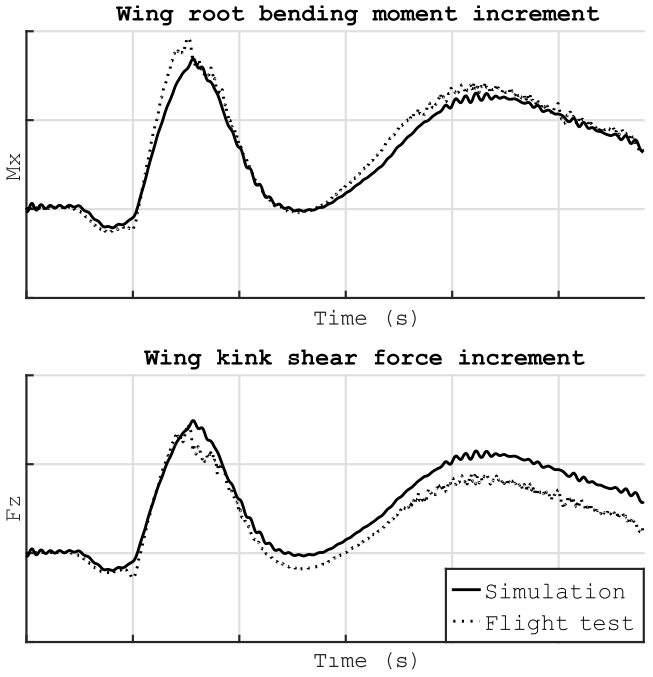

Fig. 1 Comparison of the loads during the avoidance maneuver.

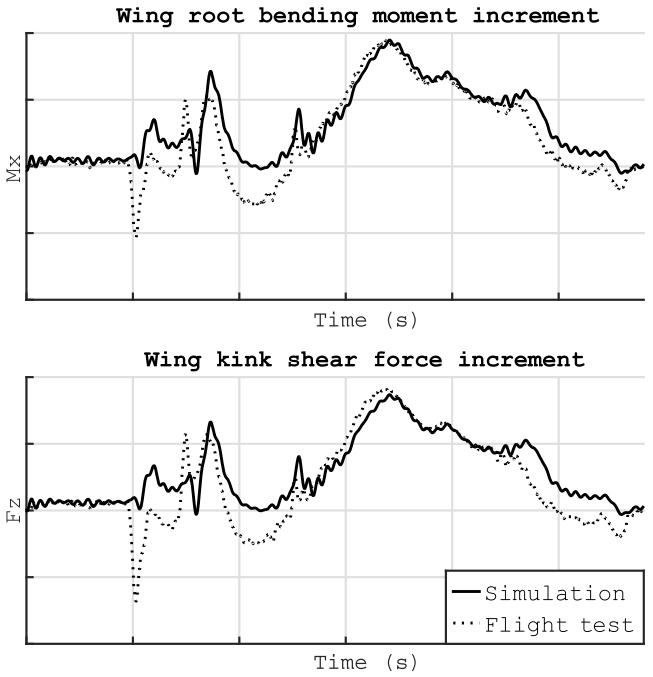

Fig. 2 Comparison of the loads during the roll maneuver.

whole duration of the maneuver, with the exception of the peak loads observed, which correspond to sudden aileron inputs followed by high roll rates.

In Fig. 3a, results from a recorded in-flight high load event are presented. The loads compared also include the actual values and not just the incremental ones. The specific incident is characterized by high vertical accelerations occurring while the aircraft was at a bank angle, combined with high lateral loads, which are not taken into account by the simulation, as no aerodynamic modeling exists along this direction. As observed in Fig. 3a, the match of the loads on the wing is reasonably good, although the 1 *g* load levels tend to be underestimated once again. Keeping into consideration that the event examined involves significant control surface deflections and lateral loads that are not taken into account by the simulation, the compared loads match adequately.

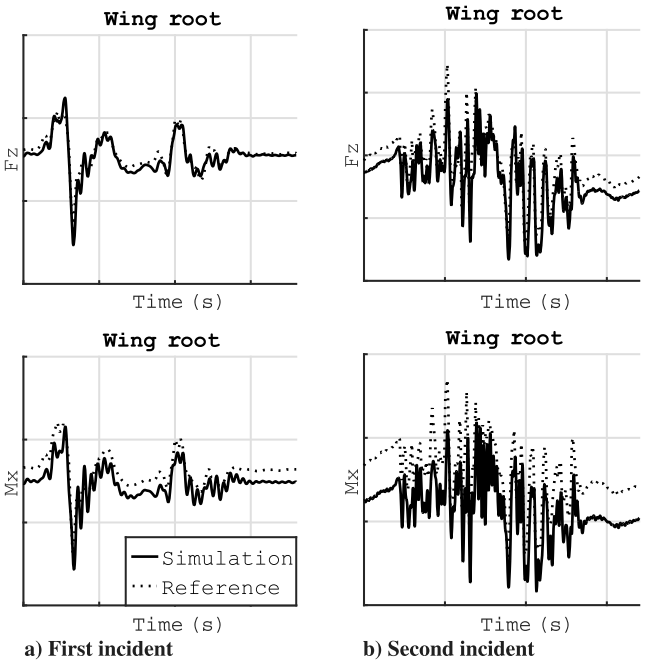

a) First incident **b) Second incident**

Fig. 3 Comparison of the loads during the two real incidents.

Table 1 Differences between loads calculated by FORTIA over the ones calculated with the simulation

Case	Wing root F_x, %	Wing root M_x, %
1	2.2	−1.0
2	7.4	−3.2
3	5.6	5.6
4	−5.9	−15.7
5	−0.8	−5.8

The second real incident case is characterized more by continuous turbulence rather than discrete gusts. This case also involves serious lateral accelerations. The conclusions drawn from this second case, as seen in Fig. 3b, do not differ compared with the ones drawn from the first case. An additional trend that is spotted is that the bending moments are more under- or overestimated compared with the shear forces.

A complete validation of FORTIA against the simulation or of FORTIA against reference data has not been conducted. That is firstly because FORTIA has not been fully developed, that is, not all mass cases have been run, and secondly, because the number of suspected high load incidents that have been recalculated with high-fidelity in-house software is limited. Nonetheless, a number of available cases are presented in Table 1. Only maximum and minimum values will be compared because FORTIA does not produce time series data as the simulation does. The differences between FORTIA and the corresponding values calculated by the simulation are expressed as percentages and have been normalized against the relevant limit loads. A positive sign means that FORTIA has overestimated the load quantity. The short list of results presented previously indicates that the extensive simplifications introduced to arrive at the LMA are not introducing significant errors.

IV. Conclusions

The presented LMA named FORTIA was specifically developed to suit the needs and particularity of a typical modern aircraft family. More specifically, FORTIA needs to be able to run on real-time onboard commercial aircraft, which are already instrumented with a set of sensors and computational systems. In general and keeping in mind the extensive simplifications introduced to keep the complexity

low, FORTIA calculates dynamic increments due to maneuvering and turbulence accurately.

More specifically, the incremental load levels produced for the root of the wing match the reference incremental values well. The only important discrepancy observed concerns the load levels at $1g$ flight conditions, which is not considered significant, as fixes can be easily implemented. An easy and straightforward fix to implement the correct $1g$ load levels for the wing (for each different mass case) in FORTIA would be to calculate those $1g$ loads through a high-fidelity simulation software. Because this $1g$ load level is just a constant parameter within FORTIA, it can be directly replaced.

References

[1] Johnston, V. G. W., and John, T., "Aircraft Load Factor Overload Warning System," U.S. Patent 4302745, Nov. 1981.

[2] Delaplace, F., Marquier, S., Mathieu, G., and Squeglia, G., "Process and Device for Detecting on an Aircraft an Overshoot of Design Loads at the Level of a Structural Part of Said Aircraft," U.S. Patent 7164366, Jan. 2007.

[3] Delaplace, F., Marquier, S., Mathieu, G., and Squeglia, G., "Method and Device for Detecting an Overstepping of Design Loads of the Fin of an Aircraft," U.S. Patent 7382283, June 2007.

[4] Reed, S. C., "Indirect Aircraft Structural Monitoring Using Artificial Neural Networks," *Aeronautical Journal*, Vol. 112, No. 1131, 2008, pp. 251–265. https://doi.org/10.1017/S0001924000002190

[5] Reed, S. C., "Development of a Parametric-Based Indirect Aircraft Structural Usage Monitoring System Using Artificial Neural Networks," *Aeronautical Journal*, Vol. 111, No. 1118, 2007, pp. 209–230. https://doi.org/10.1017/S0001924000004474

[6] Halle, M., and Thielecke, F., "Flight Loads Estimation Using Local Model Networks," *29th Congress of the International Council of the Aeronautical Sciences*, ICAS, Bonn, Germany, 2014, pp. 1–12.

[7] Halle, M., Thielecke, F., and Lindenau, O., "Comparison of Real-Time Flight Loads Estimation Methods," *CEAS Aeronautical Journal*, Vol. 5, No. 4, 2014, pp. 501–513. https://doi.org/10.1007/s13272-014-0122-3

[8] Fuentes, R., Cross, E. J., Halfpenny, A., Worden, K., and Barthorpe, R. J., "Aircraft Parametric Structural Load Monitoring Using Gaussian Process Regression," *7th European Workshop on Structural Health Monitoring*, Inria Rennes-Bretagne Atlantique, Rennes, France, 2014, pp. 1933–1940, http://hal.inria.fr/docs/01/02/20/48/PDF/0233.pdf.

[9] Bect, P., Simeu-Abazi, Z., and Lois, P., "Diagnostic and Decision Support Systems by Identification of Abnormal Events: Application to Helicopters," *Aerospace Science and Technology*, Vol. 46, Oct. 2015, pp. 339–350. https://doi.org/10.1016/j.ast.2015.07.024

[10] Azzam, H., "A Practical Approach for the Indirect Prediction of Structural Fatigue from Measured Flight Parameters," *Proceedings of the Institution of Mechanical Engineers, Part G: Journal of Aerospace Engineering*, Vol. 211, No. 1, 1997, pp. 29–38. https://doi.org/10.1243/0954410971532479

[11] Wallace, M., Azzam, H., and Newman, S., "Indirect Approaches to Individual Aircraft Structural Monitoring," *Proceedings of the Institution of Mechanical Engineers, Part G: Journal of Aerospace Engineering*, Vol. 218, No. 5, 2004, pp. 329–346. https://doi.org/10.1243/0954410042467059

[12] Manry, M. T., Hsieh, C.-H., and Chandrasekaran, H., "Near-Optimal Flight Load Synthesis Using Neural Nets," *Neural Networks for Signal Processing IX: Proceedings of the 1999 IEEE Signal Processing Society Workshop (Cat. No. 98TH8468)*, IEEE, New York, 1999, pp. 535–544. https://doi.org/10.1109/NNSP.1999.788173

[13] Azzam, H., Beaven, F., Hebden, T., Gill, L., and Wallace, M., "Fusion and Decision Making Techniques for Structural Prognostic Health Management," *2005 IEEE Aerospace Conference*, IEEE, New York, 2005, pp. 3763–3774. https://doi.org/10.1109/AERO.2005.1559683

[14] Zhu, S., and Wang, Y., "Scaled Sequential Threshold Least-Squares (S^2 TLS) Algorithm for Sparse Regression Modeling and Flight Load Prediction," *Aerospace Science and Technology*, Vol. 85, Feb. 2019, pp. 514–528. https://doi.org/10.1016/j.ast.2018.12.038

[15] Li, C., Mahadevan, S., Ling, Y., Choze, S., and Wang, L., "Dynamic Bayesian Network for Aircraft Wing Health Monitoring Digital Twin," *AIAA Journal*, Vol. 55, No. 3, 2017, pp. 930–941. https://doi.org/10.2514/1.J055201

[16] Castellani, M., Lemmens, Y., and Cooper, J., "Reduced Order Model Approach for Efficient Aircraft Loads Prediction," *SAE International Journal of Aerospace*, Vol. 8, No. 2, 2015, pp. 273–281. https://doi.org/10.4271/2015-01-2568

[17] Castellani, M., Lemmens, Y., and Cooper, J. E., "Parametric Reduced Order Model Approach for Rapid Dynamic Loads Prediction," *Aerospace Science and Technology*, Vol. 52, May 2016, pp. 29–40. https://doi.org/10.1016/j.ast.2016.02.015

[18] Castrichini, A., Cooper, J. E., Benoit, T., and Lemmens, Y., "Gust and Ground Loads Integration for Aircraft Landing Loads Prediction," *Journal of Aircraft*, Vol. 55, No. 1, 2018, pp. 184–194. https://doi.org/10.2514/1.C034369

[19] Viana, M. V. P., "Time-Domain System Identification of Rigid-Body Multipoint Loads Model," *AIAA Atmospheric Flight Mechanics Conference, AVIATION 2016*, 2016, https://elib.dlr.de/105871/.

[20] Henrichfreise, H., Bensch, L., Jusseit, J., Merz, L., and Gojny, M., "Estimation of Gusts and Structural Loads for Commercial Aircraft," *International Forum on Aeroelasticity and Structural Dynamics (IFASD)*, IFASD, 2009, pp. 1–11, http://www.dmecs.de/downloads/publications/gust-load-estimation-for-aircraft/estimation-of-gusts-and-structural-loads-for-commercial-aircraft-downlo.html?key=19fc4952c4b03c25b82294c01fc5a807a6395f58.

[21] Wright, J. R., and Cooper, J. E., *Introduction to Aircraft Aeroelasticity and Loads*, Wiley, New Jersey, 2007, pp. 27–47.

[22] Voutsinas, S. G., "Vortex Methods in Aeronautics: How to Make Things Work," *International Journal of Computational Fluid Dynamics*, Vol. 20, No. 1, 2006, pp. 3–18. https://doi.org/10.1080/10618560600566059

[23] Abbas-Bayoumi, A., and Becker, K., "An Industrial View on Numerical Simulation for Aircraft Aerodynamic Design," *Journal of Mathematics in Industry*, Vol. 1, No. 1, 2011, p. 10. https://doi.org/10.1186/2190-5983-1-10

[24] Becker, K., and Vassberg, J., *Numerical Aerodynamics in Transport Aircraft Design*, Springer, Berlin, 2009, pp. 209–220. https://doi.org/10.1007/978-3-540-70805-6_16

[25] Reschke, C., "Flight Loads Analysis with Inertially Coupled Equations of Motion," *AIAA Atmospheric Flight Mechanics Conference and Exhibit*, AIAA Paper 2005-6026, 2015. https://doi.org/10.2514/6.2005-6026

[26] Rokhsaz, K., and Kliment, L. K., "Preliminary Investigation of Flight Loads of Single-Engine Air Tankers," *Journal of Aircraft*, Vol. 53, No. 2, 2016, pp. 323–332. https://doi.org/10.2514/1.C033331

[27] Rokhsaz, K., Kliment, L. K., Terning, B. R., and Nelson, J. A., "Flight Loads Spectra of a Fleet of Heavy Air Tankers," *Journal of Aircraft*, Vol. 56, No. 5, 2019, pp. 1858–1868. https://doi.org/10.2514/1.C035424